

# Journal of Mechanics of Materials and Structures

A POSITION-AWARE LINEAR SOLID CONSTITUTIVE MODEL  
FOR PERIDYNAMICS

John A. Mitchell, Stewart A. Silling and David J. Littlewood

Volume 10, No. 5

December 2015





## A POSITION-AWARE LINEAR SOLID CONSTITUTIVE MODEL FOR PERIDYNAMICS

JOHN A. MITCHELL, STEWART A. SILLING AND DAVID J. LITTLEWOOD

A position-aware linear solid (PALS) peridynamic constitutive model is proposed for isotropic elastic solids. The PALS model addresses problems that arise, in ordinary peridynamic material models such as the linear peridynamic solid (LPS), due to incomplete neighborhoods near the surface of a body. Improved model behavior in the vicinity of free surfaces is achieved through the application of two influence functions that correspond, respectively, to the volumetric and deviatoric parts of the deformation. The model is position-aware in that the influence functions vary over the body and reflect the proximity of each material point to free surfaces. Demonstration calculations on simple benchmark problems show a sharp reduction in error relative to the LPS model.

### 1. Introduction

The peridynamic theory of solid mechanics allows for great flexibility in the development of constitutive models. In contrast to classical, local models, which rely on a kinematic description of material deformation at a point such as the deformation gradient, material models in the peridynamic theory determine pairwise force densities based on the deformations of a nonlocal family of neighboring material points [Silling 2000; Silling and Lehoucq 2010; Madenci and Oterkus 2014]. This enrichment of kinematic information greatly expands the range of possible constitutive laws. Peridynamic material models developed to date fall into one of three categories: bond-based, ordinary state-based, and non-ordinary state-based. Bond-based peridynamic models determine the pairwise force density that acts between two material points based only on the histories of those points (e.g., initial and current positions). The prototype microelastic brittle material model was the first peridynamic constitutive law to appear in the literature [Silling 2000]. This model served as the foundation for a subsequently developed bond-based plasticity model [Macek and Silling 2007]. The state-based theory for peridynamic constitutive models represents a significant generalization of the bond-based approach [Silling et al. 2007]. The theory of peridynamic states allows for constitutive models in which pairwise force densities are functions of not only the material points in question, but also the full set of material points within the nonlocal neighborhoods of those material points. State-based constitutive models in which pairwise force densities act in the direction of the corresponding bond in the deformed configuration are referred to as *ordinary* state-based models. Examples include the linear peridynamic solid (LPS) [Silling et al. 2007] and the plasticity and viscoelasticity models developed by Mitchell [2011a; 2011b]. The third class of material models, non-ordinary state-based, is comprised of constitutive models in which pairwise force densities are not restricted to act in the bond direction. The correspondence model approach, in which classical

---

*Keywords:* peridynamics, PALS, ordinary state, lps, surface effects, elastic model, nonlocal, integral equations.

(local) constitutive models are adapted for use within peridynamics, falls into this category [Silling et al. 2007; Foster et al. 2010; Tupek and Radovitzky 2014].

This study concerns the development of an ordinary, state-based constitutive model that improves upon the performance of the material models currently available in the literature. The primary motivation is the undesirable behavior of certain peridynamic material models in the vicinity of free surfaces. This difficulty appears, for example, in a peridynamic simulation of a uniaxial tension test, illustrated in Figure 1, using the LPS constitutive model and the mesh-free discretization approach of Silling and Askari [2005]. In this simulation, the displacements at the end portions of the bar are prescribed, and the forces on the grips,  $G_y$ , are computed, along with the engineering strain in the gauge,  $\epsilon$ . The Young's modulus may then be computed as

$$E = G_y / A_g \epsilon,$$

where  $A_g$  is the undeformed cross-sectional area of the bar in the vicinity of the gauge. The expected value of Young's modulus is the slope of the green curve in Figure 2. Modern three-dimensional finite element codes can accurately reproduce the Young's modulus in a simulation of the uniaxial tension test for a linear elastic material. However, a typical three-dimensional peridynamic simulation using the LPS material model predicts the red curve in Figure 2. The difference in slope between the two curves shows that the peridynamic model under-predicts the load on the grips for a given value of strain. The LPS material parameters are calibrated for points in the interior of a body and do not take into account whether a point is near a boundary [Silling et al. 2007]. Due to the nonlocality of the peridynamic equations, the LPS material model becomes inaccurate at points near a free surface. Here, some of the peridynamic bonds that would be present in the interior are missing (Figure 3). Because bonds are missing, they do not contribute to the net force on the cross-section of the gauge, hence the total force is under-predicted. While this effect manifests for a number of constitutive models, it is not present for all models; correspondence models are an exception because missing bonds are compensated for by the shape tensor  $K$ .

The under-prediction of force at material points near a free surface is often referred to as the *surface effect* in peridynamics. This effect presents a practical difficulty in applying bond-based models and ordinary state-based models such as the LPS. Approaches for mitigating the surface effect have been proposed by Kilic, Macek and Silling, and Mitchell. Following a bond-based approach, Kilic [2008] proposed a position-aware correction that is computed iteratively for each material point. Macek and Silling [2007] developed a position-aware force normalization that scales the stiffness of points near a surface using a ratio of eigenvalues from local  $3 \times 3$  stiffness matrices, where eigenvalues are computed (with the same material properties) for points near a free surface and on the interior. Mitchell [2013] developed a position-aware scaling of moduli for the LPS model, but its efficacy was found to be somewhat sensitive to complex surface geometries.

The present study proposes an alternative approach to peridynamic constitutive modeling in which model parameters at a point reflect the point's location within the body, removing the need for auxiliary surface correction techniques. This position-aware approach is a significant departure from previously developed constitutive models in that the constitutive model parameters are linked directly with the geometry of the body. The position-aware linear solid (PALS) model presented herein is an extension of the LPS model that substantially reduces the surface effect. This is accomplished by introducing

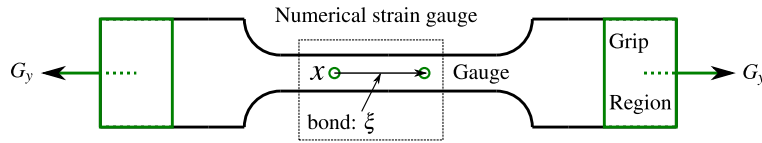


**Figure 1.** Uniaxial tension test schematic.

influence functions that are calibrated according to the bulk elastic properties at each material point, resulting in influence functions that differ for points near a free surface and points on the interior of the body. Identification of the influence functions for each point in the body is accomplished by solving a constrained minimization problem. Determination of the influence functions within a computational simulation does not require an iterative process and is instead achieved through the solution of a linear system of equations.

The present work is unique with respect to the construction and use of position-aware influence functions. As very recently pointed out by Bessa, Foster, Belytschko and Liu [Bessa et al. 2014], only constant-valued influence functions have been studied. Apparently, the two exceptions are the study by Seleson and Parks [2011] and the approach for incorporating classical damage models into state-based peridynamics by Tupek, Rimoli, and Radovitzky [Tupek et al. 2013]. Seleson and Parks used influence functions to establish relationships between bond-based and state based peridynamics models and did not consider position-aware influence functions. Influence functions developed by Tupek et al. are a product of a Gaussian and a binary valued function (0 or 1) depending upon the state of damage between two points defining a bond; this is somewhat position-aware but not in a way related to the present work.

An outline of the paper is as follows. An overview of peridynamic theory and the LPS model are given in Section 2, including calibration of the LPS parameters in the interior of a body. The influence

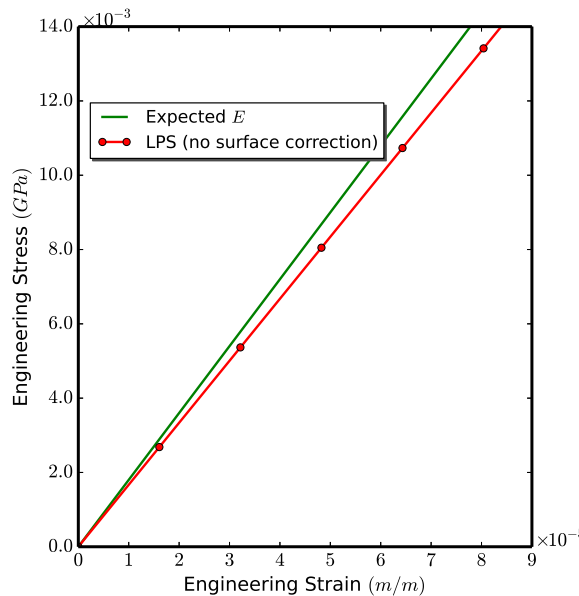


**Figure 2.** The LPS model under-predicts the Young’s modulus in a model of the uniaxial tension test.

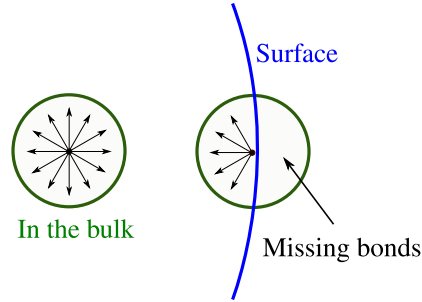


**Figure 3.** Schematic of missing peridynamic bonds.

functions used in the PALS model are derived in Section 3, followed by the formulation of the PALS force state in Section 4. The selection and usage of *matching deformations* required by the PALS model are discussed in Section 5. Section 6 presents example calculations demonstrating the efficacy of the PALS model in reducing the surface effect. Results and conclusions are given in Section 7.

## 2. Introduction to peridynamics and the LPS model

The peridynamic theory of solid mechanics [Silling 2000; Silling et al. 2007; Silling and Lehoucq 2010] is an extension of classical continuum mechanics theory [Bonet and Wood 1997]. The peridynamics extension permits discontinuities in displacements by replacing the stress divergence in the momentum equation with a volume integral

$$\rho(\mathbf{x})\ddot{\mathbf{y}}(\mathbf{x}, t) = \int_{\mathcal{B}} \mathbf{f}(\mathbf{x}', \mathbf{x}, t) dV_{\mathbf{x}'} + \mathbf{b}(\mathbf{x}, t), \quad (1)$$

where  $\mathbf{y}(\mathbf{x})$  is the current position vector of a material point  $\mathbf{x}$  at time  $t$ ,  $\rho$  is mass density in the undeformed body  $\mathcal{B}$ ,  $\mathbf{f}$  is a pairwise bond force density per unit volume,  $\mathbf{b}$  is the usual body force density, and  $\mathbf{x}'$  is an arbitrary material point within the neighborhood  $\mathcal{H}_{\mathbf{x}}$  of the point  $\mathbf{x}$ . In this section, the state-based theory of peridynamics [Silling 2000; Silling et al. 2007; Silling and Lehoucq 2010] is reviewed with emphasis on ordinary state-based constitutive models of relevance to this paper.

A *bond* vector is defined by

$$\boldsymbol{\xi} = \mathbf{x}' - \mathbf{x}, \quad 0 < |\boldsymbol{\xi}| \leq \delta,$$

where  $\delta$  is the *horizon* of the material. Conceptually,  $\delta$  is a relevant length scale and defines a spherical neighborhood  $\mathcal{H}_{\mathbf{x}}$ ; it represents the maximum distance for nonlocal interactions in the material model. Material points within the neighborhood  $\mathcal{H}_{\mathbf{x}}$  are referred to as the *family* of  $\mathbf{x}$ . It will be assumed throughout this paper that  $\delta$  is independent of  $\mathbf{x}$ .

In formulating peridynamic material models, it is convenient to use mathematical objects called *states*, which are mappings from bonds in a family to some other quantity. Vector states map bonds to vectors, and scalar states map bonds to scalars. An example of the notation used for states is as follows. The value of a vector state  $\underline{\mathbf{A}}$ , at the material point  $\mathbf{x}$  and time  $t$ , operating on a bond  $\boldsymbol{\xi}$ , is given by

$$\underline{\mathbf{A}}[\mathbf{x}, t](\boldsymbol{\xi}), \quad \mathbf{x} \in \mathcal{B}, \quad \boldsymbol{\xi} \in \mathcal{H}_{\mathbf{x}}.$$

The deformed image of a bond  $\xi = \mathbf{x}' - \mathbf{x}$  is given by the *deformation state*  $\underline{\mathbf{Y}}$ :

$$\begin{aligned}\underline{\mathbf{Y}}[\mathbf{x}, t](\xi) &= \mathbf{y}(\mathbf{x}', t) - \mathbf{y}(\mathbf{x}, t) \\ &= (\mathbf{x}' + \mathbf{u}(\mathbf{x}', t)) - (\mathbf{x} + \mathbf{u}(\mathbf{x}, t)),\end{aligned}\quad (2)$$

where  $\mathbf{u}$  is the displacement field. Further information on peridynamic states is given in [Silling et al. 2007].

The following scalar states are useful in material modeling:

- The *undeformed bond length state*  $\underline{x}$ :

$$\underline{x}(\xi) = |\xi|.$$

- The *deformed bond length state*  $|\underline{\mathbf{Y}}|$ :

$$|\underline{\mathbf{Y}}|(\xi) = |\underline{\mathbf{Y}}(\xi)|. \quad (3)$$

- The *extension state*  $\underline{e}$ :

$$\underline{e}(\xi) = |\underline{\mathbf{Y}}|(\xi) - \underline{x}(\xi). \quad (4)$$

In this paper, scalar states are underlined and written using italics, such as  $\underline{e}$ ; vector states are written using bold and underlined, as in  $\underline{\mathbf{Y}}$ .

This paper is concerned with state-based constitutive models in which the pairwise bond force density per unit volume  $\mathbf{f}(\mathbf{x}', \mathbf{x}, t)$  in (1) is given by

$$\mathbf{f}(\mathbf{x}', \mathbf{x}, t) = \underline{\mathbf{T}}[\mathbf{x}, t](\mathbf{x}' - \mathbf{x}) - \underline{\mathbf{T}}[\mathbf{x}', t](\mathbf{x} - \mathbf{x}'). \quad (5)$$

The vector state  $\underline{\mathbf{T}}[\mathbf{x}]$  is called the *force state*. In (5),  $\mathbf{f}$  contains contributions from the force states at both  $\mathbf{x}$  and  $\mathbf{x}'$  (that is, both  $\underline{\mathbf{T}}[\mathbf{x}, t]$  and  $\underline{\mathbf{T}}[\mathbf{x}', t]$ ).

In *ordinary* state-based constitutive models, the vector force state is always parallel to the deformed bond vector and written as

$$\underline{\mathbf{T}}(\xi) = \underline{t}(\xi) \underline{\mathbf{M}}(\xi), \quad (6)$$

where  $\underline{t}$  is a scalar state called the *scalar force state*, and  $\underline{\mathbf{M}}$  is a vector state that produces unit vectors parallel to the deformed bond:

$$\underline{\mathbf{M}}(\xi) = \frac{\underline{\mathbf{Y}}(\xi)}{|\underline{\mathbf{Y}}|(\xi)}. \quad (7)$$

It is assumed that deformed material points do not overlap, that is,  $\underline{\mathbf{Y}}(\xi) \neq \mathbf{0}$  for all  $\xi$ .

A *simple* material model in state-based peridynamics gives the force state as a function of the deformation state and is written  $\underline{\mathbf{T}}(\underline{\mathbf{Y}}, \mathbf{x})$ . The  $\mathbf{x}$  in this expression accounts for possible heterogeneity. All the material models considered in this paper are simple. The PALS model is inherently heterogeneous since its parameters depend on position, in particular the proximity to a free surface.

In an ordinary state-based material model, the direction of the bond force is always given by (7). Therefore, the material model is fully specified by scalar force state:  $\underline{t}(\underline{\mathbf{Y}}, \mathbf{x})$ .

The LPS model, which serves as the foundation for development of the PALS model, is summarized below.

Define the *dot product* of two scalar states  $\underline{a}$  and  $\underline{b}$  by

$$\underline{a} \bullet \underline{b} = \int_{\mathcal{K}_x} \underline{a}(\underline{\xi}) \underline{b}(\underline{\xi}) dV_{\underline{\xi}}.$$

Let  $D = 1, 2, 3$  be the number of dimensions. The *weighted volume*  $m$  and the *dilatation*  $\theta$  are scalars used in the decomposition of the extension state  $\underline{e}$  into volumetric and deviatoric parts:

$$m = (\underline{\omega x}) \bullet \underline{x}, \quad (8)$$

$$\theta = \frac{D}{m} (\underline{\omega x}) \bullet \underline{e}, \quad (9)$$

where  $\underline{\omega}$  is a scalar state called the *influence function* [Silling et al. 2007]. A key element of the constitutive model developed in this paper is the additive decomposition of the scalar extension state (4) into spherical and deviatoric parts given by

$$\underline{e} = \underline{e}^i + \underline{\varepsilon}, \quad (10)$$

where the *spherical extension state*  $\underline{e}^i$  is defined by

$$\underline{e}^i = \theta \underline{x} / D. \quad (11)$$

Using the above quantities, the *deviatoric extension state*  $\underline{\varepsilon}$  is constructed as

$$\underline{\varepsilon} = \underline{e} - \theta \underline{x} / D. \quad (12)$$

All of the above quantities are dependent on  $\underline{x}$  and  $\underline{Y}$ , but these dependencies are omitted from the notation for simplicity.

The scalar force state for the LPS model is derived from an elastic energy functional  $W$  of the form

$$W(\theta, \underline{\varepsilon}) = \frac{1}{2} \kappa \theta^2 + \frac{1}{2} \alpha \underline{\varepsilon} \bullet \underline{\omega \varepsilon}, \quad (13)$$

where  $\kappa$  is the bulk modulus and  $\alpha$  is a constant. This implies that  $\underline{t}$  is decomposed into scalar volumetric and deviatoric force states:

$$\underline{t} = \underline{t}^i + \underline{t}^d, \quad (14)$$

where

$$\underline{t}^i = \frac{\partial W}{\partial \theta} \frac{\partial \theta}{\partial \underline{e}^i}, \quad \underline{t}^d = \frac{\partial W}{\partial \underline{\varepsilon}}. \quad (15)$$

Here, the notation  $\partial/\partial \underline{a}$ , where  $\underline{a}$  is a state, refers to the Fréchet derivative [Silling et al. 2007]. The Fréchet derivative of a scalar-valued function  $\psi$  of a state  $\underline{a}$  has the property that, for a differential change  $d\underline{a}$ ,

$$d\psi = \frac{\partial \psi}{\partial \underline{a}} \bullet d\underline{a}. \quad (16)$$

Although geometrically nonlinear, the LPS model is a peridynamic analogue of Hooke's law for isotropic materials. For points  $\underline{x}$  in the interior of the body, equating the elastic energy density from the LPS material with the strain energy density from the local theory leads to the calibration (for  $D = 3$ )

$$\alpha = 15\mu/m,$$



where  $\mu$  is the conventional shear modulus from the local theory and  $m$  is given by (8). The above relation for  $\alpha$  is inaccurate for points near a free surface. Experience with the LPS model in complex geometries suggests that a simple correction to  $\alpha$  near free surfaces [Mitchell 2013] is not general enough, motivating the PALS model.

Using (15), the scalar force state for the LPS model takes the form

$$\underline{t} = \frac{D\kappa\theta}{m}\underline{\omega x} + \alpha\underline{\omega\varepsilon}. \tag{17}$$

Observe that the scalar force state contains independent terms that depend on either the isotropic or deviatoric part of the extension state.

An important side note relates to the use of (9) and (12) for cases when  $D = 1$  or  $2$ ; conditions of uniaxial stress and plane stress are local concepts which do not precisely exist in peridynamics, although practical and useful analogies exist. In particular, (9) and (12) remain valid for these and other conditions although care must be taken with respect to the choice of material parameters. The correct parameters are found by assuming appropriate homogeneous deformations and equating the local energy density with the peridynamic energy density.

### 3. PALS model and selection of influence functions

The PALS concept proposed in this paper is a kinematic correction to the dilatation and deviatoric extension states and circumvents the surface effect under a wide range of conditions. It also helps to reduce errors introduced by spatial discretizations.

The basic idea is to introduce a set of constraints and associated Lagrange multipliers which force the dilatation and deviatoric extension states to reproduce a set of predetermined deformations called *matching deformations*. Using this set of matching deformations, two linear problems (one for dilatation and one for deviatoric extension) are defined for each point; the solution to these linear problems gives two sets of Lagrange multipliers that determine the influence functions  $\underline{\omega}(\xi)$  and  $\underline{\sigma}(\xi)$ . In general, these influence functions are unique for each material point within the body; they determine the dilatation and deviatoric extension state for any deformation; importantly, they reflect the position and proximity of the point to free surfaces. Both  $\underline{\omega}$  and  $\underline{\sigma}$  depend on  $\mathbf{x}$ , although this dependence is omitted from the notation in the following discussion.

In the remainder of this article, the following linear approximation to the extension state will be used:

$$\underline{e}(\xi) = \frac{\xi \cdot \underline{U}(\xi)}{|\xi|}, \quad \underline{U}(\xi) = \underline{Y}(\xi) - \xi \quad \text{for all } \xi \in \mathcal{H}_x. \tag{18}$$

The vector state  $\underline{U}$  is called the *displacement state*.

In the PALS model, the elastic energy density at a point  $\mathbf{x}$  is defined by

$$W(\theta, \underline{\varepsilon}) = \frac{1}{2}\kappa\theta^2 + \mu(\underline{\sigma\varepsilon}) \bullet \underline{\varepsilon}, \tag{19}$$

where  $\mu$  is the shear modulus and  $\underline{\varepsilon}$  is defined in (12);  $\underline{\sigma}$  is a new influence function called the *deviatoric influence function*. The dilatation  $\theta$  is defined using the extension state  $\underline{e}$  by

$$\theta = (\underline{\omega x}) \bullet \underline{e}, \tag{20}$$

where  $\underline{\omega}$  is normalized such that the weighted volume  $m$  used in the LPS is not needed (that is,  $m = D$ ). The new influence function  $\underline{\omega}$  is constructed starting from a given influence function  $\underline{\omega}^0$  which is arbitrary. Typically, one assumes that  $\underline{\omega}^0$  follows some convenient dependence on bond length such as a constant or a Gaussian.

Assume that a set of displacement gradient tensors  $\mathbf{H}^1, \mathbf{H}^2, \dots, \mathbf{H}^K$  are given — these are the *matching deformations*. The new influence function  $\underline{\omega}$  is constructed as a best approximation to  $\underline{\omega}^0$  subject to constraints which ensure the dilatation for each of the matching deformations is reproduced exactly;  $\underline{\omega}$  is determined such that the dilatation induced by each  $\mathbf{H}^k$  and evaluated using (18) and (20) equals the trace of the matching deformation  $\mathbf{H}^k$ . Note that there are no symmetry requirements on the matching deformations; this will become even more apparent in the construction of the deviatoric influence function.

Assume that a scalar state  $\underline{\omega}^0$  is given, and let  $\lambda^1, \lambda^2, \dots, \lambda^K$  be Lagrange multipliers — one for each matching deformation  $\mathbf{H}^k$ . To find  $\underline{\omega}$ , define a functional  $I$  by

$$I(\underline{\omega}, \lambda^1, \dots, \lambda^K) = \frac{1}{2}(\underline{\omega} - \underline{\omega}^0) \bullet (\underline{\omega} - \underline{\omega}^0) - \sum_{k=1}^K \lambda^k [(\underline{\omega} \underline{x}) \bullet \underline{e}^k - \text{trace } \mathbf{H}^k], \quad (21)$$

where the linear extension states  $\underline{e}^k$  (see (18)) are defined using the matching deformations  $\mathbf{H}^k$  by

$$\underline{e}^k \langle \underline{\xi} \rangle = \frac{\underline{\xi} \cdot (\mathbf{H}^k \underline{\xi})}{|\underline{\xi}|} \quad \text{for all } \underline{\xi} \in \mathcal{H}_x. \quad (22)$$

It is required that  $I$  be stationary with respect to  $\underline{\omega}$  and  $\lambda^1, \dots, \lambda^K$ . Taking the first variation of  $I$  leads to

$$\delta I = \frac{\partial I}{\partial \underline{\omega}} \bullet \delta \underline{\omega} + \sum_{k=1}^K \frac{\partial I}{\partial \lambda^k} \delta \lambda^k, \quad (23)$$

where  $\partial I / \partial \underline{\omega}$  denotes the Fréchet derivative of  $I$  with respect to  $\underline{\omega}$ . Observe that, for a given  $k$ ,  $1 \leq k \leq K$ ,

$$\frac{\partial I}{\partial \lambda^k} = 0 \quad \Rightarrow \quad (\underline{\omega} \underline{x}) \bullet \underline{e}^k = \text{trace } \mathbf{H}^k, \quad (24)$$

which means the state  $\underline{\omega}$  exactly reproduces the dilatations in the matching deformations. Furthermore, referring to the first term on the right-hand side of (21), this  $\underline{\omega}$  approximates the desired  $\underline{\omega}^0$  in the least squares sense. Evaluating the Fréchet derivative of the right-hand side of (21) with respect to  $\underline{\omega}$  gives

$$\frac{\partial I}{\partial \underline{\omega}} = 0 \quad \Rightarrow \quad \underline{\omega} = \underline{\omega}^0 + \sum_{k=1}^K \lambda^k \underline{x} \underline{e}^k. \quad (25)$$

This relation reveals the structure of  $\underline{\omega}$ : it differs from  $\underline{\omega}^0$  by a linear combination of the states  $\underline{x} \underline{e}^k$ ,  $k = 1, 2, \dots, K$ . To evaluate the  $\lambda^k$  explicitly, impose the  $K$  requirements from the matching deformations using (25):

$$\begin{aligned} \text{trace } \mathbf{H}^k &= (\underline{\omega} \underline{x}) \bullet \underline{e}^k = \left[ \left( \underline{\omega}^0 + \sum_{n=1}^K \lambda^n \underline{x} \underline{e}^n \right) \underline{x} \right] \bullet \underline{e}^k \\ &= (\underline{\omega}^0 \underline{x}) \bullet \underline{e}^k + \sum_{n=1}^K \lambda^n (\underline{x} \underline{e}^n) \bullet (\underline{x} \underline{e}^k), \quad k = 1, 2, \dots, K. \end{aligned} \quad (26)$$

This is a nonhomogeneous linear algebraic system with unknowns  $\lambda^1, \lambda^2, \dots, \lambda^K$ . The solution to this system, together with (25), provides the desired influence function  $\underline{\omega}$  within a constant scale factor  $c$ . For consistency with the decomposition of the extension state (see (10)–(12))  $c$  is chosen so that

$$(c\underline{\omega}\underline{x}) \bullet \underline{x} = D. \quad (27)$$

Now consider the deviatoric part of the strain energy. In the PALS model, as in the LPS model, this is treated by summing the energies in the deviatoric bond extensions. Motivated by the stored elastic energy density function in (19), it is convenient to express the deviatoric contribution in terms of the *total shear* defined by

$$\gamma = (\underline{\sigma}\underline{\varepsilon}) \bullet \underline{\varepsilon}, \quad (28)$$

thus, from (19),

$$W = \frac{1}{2}\kappa\theta^2 + \mu\gamma. \quad (29)$$

Recall that, in the classical theory, for any displacement gradient  $\mathbf{H}$ ,

$$W = \frac{1}{2}\kappa\theta^2 + \mu \text{trace}[\text{dev sym } \mathbf{H}]^T [\text{dev sym } \mathbf{H}]. \quad (30)$$

The deviatoric tensor in this expression is the deviatoric strain tensor:

$$\epsilon^d = \text{dev sym } \mathbf{H}, \quad \epsilon_{ij}^d = \frac{1}{2}(H_{ij} + H_{ji}) - \frac{H_{kk}\delta_{ij}}{D}. \quad (31)$$

Combining (28)–(30) provides the requirement on  $\underline{\sigma}$  that, for any of the matching deformations  $\mathbf{H}^k$ ,

$$(\underline{\sigma}\underline{\varepsilon}^k) \bullet \underline{\varepsilon}^k = \text{trace}[\text{dev sym } \mathbf{H}^k]^T [\text{dev sym } \mathbf{H}^k]. \quad (32)$$

Suppose a reference influence function  $\underline{\sigma}^0$  is given. Proceeding as with the dilatational contribution, define a functional  $N(\underline{\sigma}, \tau^1, \dots, \tau^K)$  by

$$N(\underline{\sigma}, \tau^1, \dots, \tau^K) = \frac{1}{2}(\underline{\sigma} - \underline{\sigma}^0) \bullet (\underline{\sigma} - \underline{\sigma}^0) - \sum_{k=1}^K \tau^k [(\underline{\sigma}\underline{\varepsilon}^k) \bullet \underline{\varepsilon}^k - \gamma^k], \quad (33)$$

where  $\tau^1, \tau^2, \dots, \tau^K$  are Lagrange multipliers,

$$\gamma^k := \text{trace}[\text{dev sym } \mathbf{H}^k]^T [\text{dev sym } \mathbf{H}^k], \quad (34)$$

and

$$\underline{\varepsilon}^k = \underline{e}^k - (\text{trace } \mathbf{H}^k)\underline{x}/D. \quad (35)$$

The influence function  $\underline{\sigma}$  and the associated Lagrange multipliers are found by taking the first variation of (33):

$$\delta N = \frac{\partial N}{\partial \underline{\sigma}} \bullet \delta \underline{\sigma} + \sum_{k=1}^K \frac{\partial N}{\partial \tau^k} \delta \tau^k. \quad (36)$$

Requiring  $N$  to be stationary,

$$\frac{\partial N}{\partial \tau^k} = 0 \quad \Rightarrow \quad (\underline{\sigma}\underline{\varepsilon}^k) \bullet \underline{\varepsilon}^k = \gamma^k \quad (37)$$

and

$$\frac{\partial N}{\partial \underline{\sigma}} = 0 \quad \Rightarrow \quad \underline{\sigma} = \underline{\sigma}^0 + \sum_{k=1}^K \tau^k \underline{\varepsilon}^k \underline{\varepsilon}^k. \quad (38)$$

This leads to the following nonhomogeneous linear algebraic system with unknowns  $\tau^k$ :

$$\gamma^k = (\underline{\sigma}^0 \underline{\varepsilon}^k) \bullet \underline{\varepsilon}^k + \sum_{n=1}^K \tau^n (\underline{\varepsilon}^n \underline{\varepsilon}^n) \bullet (\underline{\varepsilon}^k \underline{\varepsilon}^k), \quad k = 1, 2, \dots, K. \quad (39)$$

When taken with (38), the  $\tau^n$  values that solve this system give the  $\underline{\sigma}$  states for the PALS model at a given point  $\mathbf{x}$ .

Except for the interior of the body, where the neighborhood  $\mathcal{H}_{\mathbf{x}}$  does not intersect with the free surface,  $\lambda^n$  and  $\tau^n$  depend on  $\mathbf{x}$ . Because this calibration varies from point to point, the model is *position aware*. In summary, the PALS model is calibrated at each  $\mathbf{x}$  by the following steps:

- (1) Define initial guesses for  $\underline{\omega}^0$  and  $\underline{\sigma}^0$ .
- (2) Choose  $K$  linearly independent displacement gradient tensors  $\mathbf{H}^1, \dots, \mathbf{H}^K$ . (In three dimensions, we choose  $K = 6$  because there are at most 6 linearly independent strain tensors.)
- (3) Solve the  $K \times K$  linear algebraic system given by (26) for  $\lambda^1, \dots, \lambda^K$ .
- (4) Find  $\underline{\omega}$  from (25) and normalize according to (27).
- (5) Solve the  $K \times K$  linear algebraic system given by (39) for  $\tau^1, \dots, \tau^K$ .
- (6) Find  $\underline{\sigma}$  from (38).

In general, values of  $\underline{\omega}(\xi)$  and  $\underline{\sigma}(\xi)$  may be negative for some bonds in the family. This is acceptable and does not lead to material instability, since it does not necessarily imply imaginary wave speeds [Silling and Lehoucq 2010].

In a computational implementation, it is sufficient to evaluate and store the  $2K$  Lagrange multipliers (for each node in the discretization) at the start of a run and, on the fly, compute influence functions as they are needed. This uses less memory (but requires more floating point operations) than saving influence function values on each bond for every point. The cost of evaluating one of the two PALS model influence functions is very similar to the cost of evaluating the LPS model influence function, although it requires retrieval and use of  $K$  Lagrange multiplier values for each point.

The cost/benefit analysis of using the PALS model is problem-dependent and relates to the domain geometry and the ratio of surface area to volume. Since peridynamics is fundamentally oriented towards fracture, it is likely that surface effects increase as new surfaces are created with each fracture. If bonds are broken during a simulation, the PALS model influence functions should be recomputed subject to a cost/benefit analysis which is beyond the scope of this paper. Simple engineering demonstration calculations later in this paper were chosen which highlight the degree to which surface effects can degrade the LPS model; in these cases the PALS model substantially reduces the surface effect.

#### 4. PALS scalar force state

In the preceding section, the influence functions  $\underline{\omega}$  and  $\underline{\sigma}$  were determined. Now we evaluate the bond forces using these influence functions. Recall that the strain energy density is given by (19).

The scalar force state  $\underline{t}$  is found from the Fréchet derivative of  $W$  with respect to  $\underline{e}$ :

$$\underline{t} = \frac{\partial W}{\partial \underline{e}}.$$

To evaluate  $\underline{t}$  explicitly, consider a change in the elastic energy density due to a small change  $\underline{\Delta e}$  in the extension state and use (16):

$$\frac{\partial W}{\partial e} \bullet \underline{\Delta e} = \underline{t} \bullet \underline{\Delta e}. \tag{40}$$

Using (12), (19), and (20) for the PALS stored elastic energy density  $W$ , the change  $\Delta W$  is explicitly evaluated as

$$\begin{aligned} \underline{t} \bullet \underline{\Delta e} = \Delta W &= \kappa \theta \underline{\omega x} \bullet \underline{\Delta e} + 2\mu \underline{\sigma \varepsilon} \bullet \left( \underline{\Delta e} - \frac{\Delta \theta x}{D} \right) \\ &= \left[ \left( \kappa \theta - \frac{2\mu}{D} \underline{\sigma \varepsilon} \bullet x \right) \underline{\omega x} + 2\mu \underline{\sigma \varepsilon} \right] \bullet \underline{\Delta e}. \end{aligned} \tag{41}$$

From this, the scalar force state  $\underline{t}$  is directly identified as

$$\underline{t} = \left( \kappa \theta - \frac{2\mu}{D} (\underline{\sigma x}) \bullet \underline{\varepsilon} \right) \underline{\omega x} + 2\mu \underline{\sigma \varepsilon}. \tag{42}$$

The term involving  $(\underline{\sigma x}) \bullet \underline{\varepsilon}$  appears because different influence functions  $\underline{\omega}$  and  $\underline{\sigma}$  are used for the dilatational and deviatoric terms in the elastic energy density. If  $\underline{\omega} \equiv \underline{\sigma}$ , then this term vanishes, as in the LPS model. The (vector) force state is found from (6).

### 5. Matching deformations

The PALS model development in Section 3 was generic with respect to the use of specific matching deformations  $\mathbf{H}^1, \mathbf{H}^2, \dots, \mathbf{H}^K$ . In this section, a sample set of matching deformations is provided. The matching deformations provided here were used in the example problems described in the next section; they are expected to provide good results in general, although alternative choices are possible. When  $D = 3$  (three dimensions), the local theory strain tensor has 6 independent components, hence we choose  $K = 6$  matching deformations. The strain components will be denoted  $XX, YY, ZZ, XY, XZ, YZ$ . The matching deformations (shown below) represent three deformations for uniaxial strain and three for simple shear:

$$\mathbf{H}^1 = \begin{bmatrix} XX & 0 & 0 \\ 0 & 0 & 0 \\ 0 & 0 & 0 \end{bmatrix}, \quad \mathbf{H}^2 = \begin{bmatrix} 0 & 0 & 0 \\ 0 & YY & 0 \\ 0 & 0 & 0 \end{bmatrix}, \quad \mathbf{H}^3 = \begin{bmatrix} 0 & 0 & 0 \\ 0 & 0 & 0 \\ 0 & 0 & ZZ \end{bmatrix}, \tag{43}$$

$$\mathbf{H}^4 = \begin{bmatrix} 0 & XY & 0 \\ XY & 0 & 0 \\ 0 & 0 & 0 \end{bmatrix}, \quad \mathbf{H}^5 = \begin{bmatrix} 0 & 0 & XZ \\ 0 & 0 & 0 \\ XZ & 0 & 0 \end{bmatrix}, \quad \mathbf{H}^6 = \begin{bmatrix} 0 & 0 & 0 \\ 0 & 0 & YZ \\ 0 & YZ & 0 \end{bmatrix}. \tag{44}$$

Let  $(a, b, c)$  be components of a bond vector  $\xi$  and let  $|\xi|$  denote its length. It is convenient to set the magnitudes of the strain components  $XX, \dots, YZ$  all equal to the same small positive number  $\Delta$ . Using (18), the extension states  $\underline{e}^k$  are computed, one for each matching deformation:

$$\underline{e}^1 = \frac{\Delta a^2}{|\xi|}, \quad \underline{e}^2 = \frac{\Delta b^2}{|\xi|}, \quad \underline{e}^3 = \frac{\Delta c^2}{|\xi|}, \quad \underline{e}^4 = \frac{2ab\Delta}{|\xi|}, \quad \underline{e}^5 = \frac{2ac\Delta}{|\xi|}, \quad \underline{e}^6 = \frac{2bc\Delta}{|\xi|}. \tag{45}$$

These extension states are used to form the symmetric  $6 \times 6$  matrix associated with the linear problems defined in (26) and (39). Entries in the matrix are evaluated using a quadrature scheme that is consistent

with the discretized form of the momentum equation. For example, if the mesh-free approach of Silling and Askari [2005] is employed, then dot products between state  $\underline{a}$  and  $\underline{b}$  are approximated by

$$\underline{a} \cdot \underline{b} = \int_{\mathcal{H}_x} \underline{a}(\underline{\xi}) \underline{b}(\underline{\xi}) dV_{\xi} \approx \sum_j \underline{a}_j \underline{b}_j V_j,$$

where  $j$  is a node number,  $V_j$  is its associated volume in the undeformed configuration, and  $\underline{a}_j$  and  $\underline{b}_j$  denote the value of the states  $\underline{a}$  and  $\underline{b}$  acting on the  $j$ -th bond (associated with node  $j$ ).

In the remainder of this section, specific details are given for dilatation and shear. For the matching deformations given above, components of the right-hand side vector associated with the linear problems are given. It is shown that the Lagrange multipliers,  $\lambda^k$  and  $\tau^k$  are independent of  $\Delta$  (magnitude of the strain components implied by the matching deformations).

**5.1. Dilatation influence function.** As a starting point for computing the dilatation influence function  $\underline{\omega}$  at a point, a reference influence function  $\underline{\omega}^0$  is assumed to be given. Then, using the definitions for  $\underline{e}^n$  defined in (45), it is helpful to define a scaled set of states  $\hat{\underline{e}}^n$  as

$$\underline{e}^n = \frac{\Delta \hat{\underline{e}}^n}{|\underline{\xi}|}. \quad (46)$$

Using this expression for the matching states, the linear problem defined in (26) is written as

$$\Delta^2 \sum_{k=1}^K (\hat{\underline{e}}^n \cdot \hat{\underline{e}}^k) \lambda^k = \text{trace}(\mathbf{H}^n) - \Delta \underline{\omega}^0 \cdot \hat{\underline{e}}^n, \quad (47)$$

where  $K = 6$  equations are generated by  $n = 1, 2, \dots, K$ . Because each  $\mathbf{H}^n$  is proportional to the applied deformation  $\Delta$ , the Lagrange multipliers  $\lambda^n$  are inversely proportional to  $\Delta$ . The linear problem in (47) can be rewritten as

$$\Delta^2 [K_{\lambda}] \{\lambda\} = \Delta \{\hat{R}\}, \quad (48)$$

where  $[K_{\lambda}]$  denotes the  $6 \times 6$  matrix implied by (26) and (47),  $\{\lambda\}$  denotes the unknown array of six Lagrange multiplier values, and  $\{\hat{R}\}$  denotes the right-hand side array of components defined in (47). Solving the scaled system gives the Lagrange multipliers as

$$\{\lambda\} = \{\hat{\lambda}\} / \Delta,$$

where  $\{\hat{\lambda}\} = [K_{\lambda}]^{-1} \{\hat{R}\}$ . Based upon the matching deformations ((43) and (44)) and the corresponding extension states given in (45), the dilatation influence function takes the form

$$\underline{\omega} = \underline{\omega}^0 + \sum_{k=1}^K \hat{\lambda}^k \hat{\underline{e}}^k = \underline{\omega}^0 + \hat{\lambda}^1 a^2 + \hat{\lambda}^2 b^2 + \hat{\lambda}^3 c^2 + 2\hat{\lambda}^4 ab + 2\hat{\lambda}^5 ac + 2\hat{\lambda}^6 bc. \quad (49)$$

As a final step, the above influence function is normalized according to (27).

**5.2. Deviatoric influence function.** The procedure used to compute the deviatoric Lagrange multipliers is analogous to the procedure for computing the dilatation Lagrange multipliers. The deviatoric Lagrange multipliers are computed using the linear problem defined in (39). Using the matching deformations provided in this section, the deviatoric extension states  $\underline{\varepsilon}^k$  defined in (35) take the following specific form:

$$\underline{\varepsilon}^1 = \underline{e}^1 - \frac{1}{3}\Delta|\xi|, \quad \underline{\varepsilon}^2 = \underline{e}^2 - \frac{1}{3}\Delta|\xi|, \quad \underline{\varepsilon}^3 = \underline{e}^3 - \frac{1}{3}\Delta|\xi|, \quad \underline{\varepsilon}^4 = \underline{e}^4, \quad \underline{\varepsilon}^5 = \underline{e}^5, \quad \underline{\varepsilon}^6 = \underline{e}^6. \quad (50)$$

Observe that the matching deviatoric extension states vary linearly with  $\Delta$  so that a set of scaled deviatoric extension states can be defined as  $\underline{\varepsilon}^k = \Delta \hat{\underline{\varepsilon}}^k$ . The linear problem in (39) can be rewritten as

$$\Delta^4[K_\tau]\{\tau\} = \Delta^2\{\hat{R}\}. \quad (51)$$

Solving the scaled system gives the Lagrange multipliers as

$$\{\tau\} = \{\hat{\tau}\}/\Delta^2,$$

where  $\{\hat{\tau}\} = [K_\tau]^{-1}\{\hat{R}\}$ . Based upon the matching deformations ((43) and (44)) and the corresponding extension states given in (50), the deviatoric influence function takes the form

$$\underline{\sigma} = \underline{\sigma}^0 + \sum_{k=1}^K \hat{\tau}^k \hat{\underline{\varepsilon}}^k \hat{\underline{\varepsilon}}^k, \quad (52)$$

where  $\underline{\sigma}^0$  is the given reference influence function.

## 6. Demonstration calculations

Computational simulation results are presented below for the purpose of comparing the performance of the PALS model against the LPS model. Results for a beam in tension, a hollow cylinder subjected to torsional loading, and a tensile test simulation for material characterization are given. The simulations were carried out using the *Peridigm* [Parks et al. 2012; Peridigm 2014] code following the mesh-free method of Silling and Askari [2005]. All demonstration calculations are three-dimensional and results were obtained by solving the momentum equation under conditions of static equilibrium. The *Cubit* code [Cubit 2014] was utilized to generate the discretization, and the *Paraview* code [ParaView 2014] was used for visualization of results. For further discussion of the numerical solution procedure, see [Silling and Askari 2005] and [Littlewood  $\geq$  2015].

**6.1. Square beam in tension.** This demonstration calculation is a simpler version of the tensile test described in the introduction (Section 1). A known/measured value for Young’s modulus  $E$  is given and a simple peridynamics calculation is conducted to recover  $E$  and verify the efficacy of the PALS model. In this calculation (schematic shown in Figure 4), one end of the beam is fixed while the other end has a prescribed small displacement  $u_0$ ; Dirichlet boundary conditions are applied to the end sections (shown in green) as  $u(z) = zu_0/L$ , where  $z$  is an axial coordinate with an origin  $z = 0$  centered in one of the green sections. The equilibrium solution for the displacement field is computed and reaction forces  $P$  are calculated as a post-processing step. From elementary mechanics of materials, the reaction force is

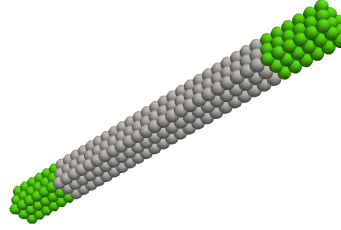


**Figure 4.** Schematic of square beam for verification of Young's modulus.

related to the applied displacement and geometric properties of the beam:

$$P = \frac{AE}{L} u_0, \quad (53)$$

where  $A = b^2$  denotes the cross-sectional area of the beam, and  $L$  denotes the length of the beam. Material and geometric properties used for these calculations are given in Tables 1 and 2. The horizon parameter  $\delta = 3.1h$  was used, where  $h = b/n$  is the mesh spacing, and  $n$  is the number of nodes along one axis of the cross-section. Graphical results for these calculations are shown in Figure 5. Error in the effective value of Young's modulus (slope of the stress-strain curve) is shown in Table 3 for a few different numerical mesh discretizations. The table gives results for two types of initial influence functions:

- Constant:

$$\underline{\omega}^0(\xi) = \underline{\sigma}^0(\xi) = 1.$$

- Gaussian:

$$\underline{\omega}^0(\xi) = \underline{\sigma}^0(\xi) = G(\delta, \xi) = e^{-|\xi|^2/\delta^2}.$$

Although oscillations are observed in the PALS results shown, the PALS model errors are substantially less than those of the LPS model for all discretizations.

**6.2. Twist test.** The focus of this example is on recovering the shear modulus  $\mu$ . In this calculation,  $\mu$  is estimated by applying an angle of twist  $\phi$  to a circular hollow cylinder. A schematic of the cylinder is depicted in Figure 6; material and geometric properties used in the calculations are given in Tables 1 and 4.

Under the assumptions that every cross-section of the cylinder remains plane and undistorted and that the material remains linearly elastic, the relationship between the angle of twist  $\phi$  and the applied

Property	Value	Units
Bulk modulus: $k$	$1.5 \times 10^{12}$	dyne/cm <sup>2</sup>
Shear modulus: $\mu$	$6.923 \times 10^{11}$	dyne/cm <sup>2</sup>

**Table 1.** Isotropic elastic material properties.

Property	Value	Units
Edge length: $b$	0.5	cm
Length: $L$	5.0	cm

**Table 2.** Square beam geometric properties. See Figure 4.



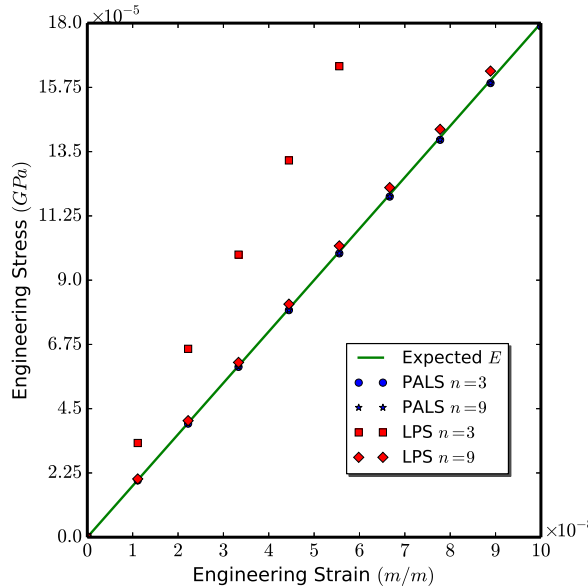


**Figure 5.** Computed stress-strain curves for the square beam in tension (Figure 4). The slope represents the effective Young’s modulus in the computational model.

torque  $T$  is

$$T = \mu J \phi / L, \tag{54}$$

where  $J$  is the area polar moment of inertia of the cross-section, and  $L$  is the length of the cylinder. Dirichlet boundary conditions are applied on points depicted in green (see Figure 6). The angles of twist applied at the ends are

$$\phi(0) = 0, \quad \phi(L) = \phi_L.$$

The expected angle of twist on any cross-section with axial position  $z$  is  $\phi(z) = z\phi_L/L$ . The computational model finds a resultant torque  $T$  from which  $\mu$  is recovered using (54). A relative error for recovery of the shear modulus  $\mu$  is computed. This error is calculated as  $(\hat{\mu} - \mu)/\mu$ , where  $\hat{\mu}$  was estimated from the PALS or LPS models using (54), and  $\mu$  is the input value given in Table 1. For these calculations, the horizon parameter  $\delta = 3.1h$  was used, where  $h = (r_o - r_i)/n$ , and  $n$  is the number of nodes through the thickness of the cylinder.

Mesh	PALS		LPS	
	$\underline{\omega}^0 = \underline{\sigma}^0 = 1$	$\underline{\omega}^0 = \underline{\sigma}^0 = G(\delta, \xi)$	$\underline{\omega}^0 = 1$	$\underline{\omega}^0 = G(\delta, \xi)$
3	0.00621	0.00621	0.649	0.649
5	0.000686	0.000685	0.173	0.173
7	0.00820	0.0082	0.0723	0.0723
9	0.00595	0.00595	0.0201	0.0201

**Table 3.** Relative error in the computed Young’s modulus for a beam under uniaxial tension.

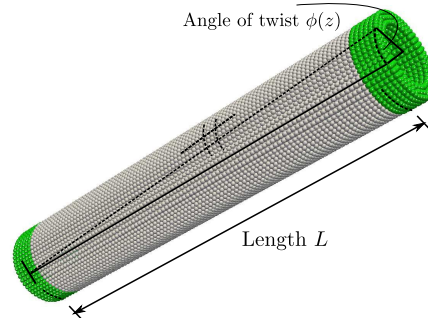


**Figure 6.** Schematic of twist test for verification of shear modulus.

Numerical results of demonstration calculations are given in Table 5 for a few different mesh discretizations. This is a particularly challenging problem because the expected solution is not a homogeneous (affine) deformation since the shear strain depends on the radial coordinate; relatedly, the local elastic energy density is independent of the axial coordinate  $z$  and varies quadratically as a function of the radial coordinate; this is shown in Figure 7 for the finest discretization,  $n = 9$ , as listed Table 5. The PALS model influence functions were computed at each point using affine matching deformations, so good results are not guaranteed by this particular choice of matching deformations. Nevertheless, the PALS model continues to show a significant reduction in error with respect to the LPS model. Better accuracy with the PALS model would be expected for thinner walled tubes, since the deformation would more closely approximate simple shear.

Several additional points are made with respect to Figure 7. This plot shows the spatial variation of the elastic energy density for any cross-section along the axis of the cylinder. Each color bar is scaled using the local analytic minimum and maximum values. Tick labels on color bars for LPS and PALS are the minimum and maximum values computed while tick labels for the local analytic calculation are the

Property	Value	Units
Inner radius: $r_i$	0.667	cm
Outer radius: $r_o$	1.0	cm
Length $L$	5.0	cm

**Table 4.** Twist test geometric parameters.

Mesh	PALS		LPS	
	$\underline{\omega}^0 = \underline{\sigma}^0 = 1$	$\underline{\omega}^0 = \underline{\sigma}^0 = G(\delta, \xi)$	$\underline{\omega}^0 = 1$	$\underline{\omega}^0 = G(\delta, \xi)$
3	0.097	0.097	0.303	0.276
5	0.056	0.056	0.168	0.158
7	0.040	0.040	0.131	0.121
9	0.026	0.026	0.117	0.107

**Table 5.** Relative error in the computed shear modulus  $\mu$  for the twist test example.

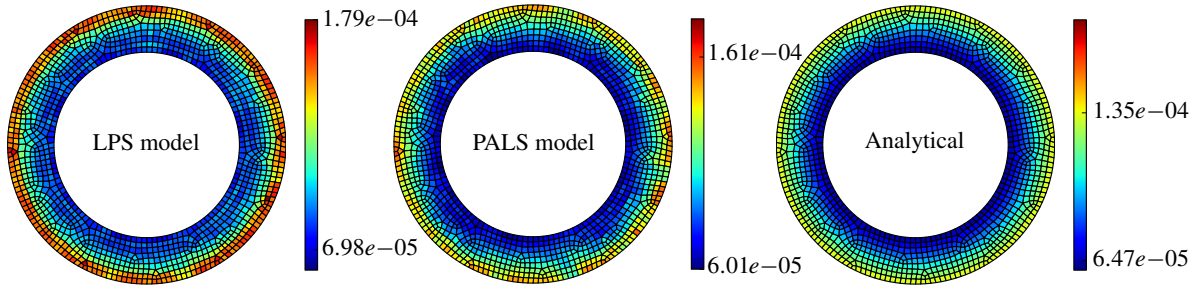


**Figure 7.** Elastic energy density for twist test calculation using LPS and PALS;  $\underline{\omega}^0 = \underline{\sigma}^0 = G(\delta, \xi)$ .

exact minimum and maximum values. As shown, the PALS model resolves the spatial variation of the energy density better than the LPS model. As previously mentioned, these calculations were done using *Peridigm* [Parks et al. 2012; Peridigm 2014]; in preparation for running *Peridigm*, the geometry of the domain is first discretized (in this case with hexahedra); for each hexahedron an equivalent peridynamic nodal volume is created and located at its centroid; although the plots in Figure 7 show a quadrilateral discretization (which corresponds to a cross-sectional view of hexahedra), this is only for plotting convenience. All calculations were fully 3D using the mesh-free method [Silling and Askari 2005].

**6.3. Tension test.** As a final demonstration calculation, the PALS model is applied to the motivation problem described in Section 1 (see Figure 1). A full three-dimensional model of the specimen was used. Improved accuracy in reproducing  $E$  using the PALS model, compared with the LPS model, is shown in Figure 8.

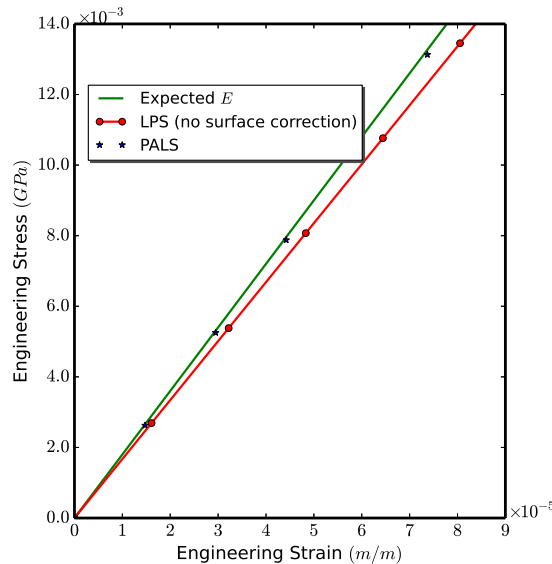


**Figure 8.** Stress-strain curve for a full 3D peridynamic model of the uniaxial tension test with PALS and LPS; both on the same discretization.

## 7. Summary and conclusions

A new position aware linear solid (PALS) model for peridynamics was introduced. The PALS model is an ordinary-state-based peridynamics constitutive model that addresses inaccuracies in previous models, most notably the linear peridynamic solid (LPS) [Silling et al. 2007], due to the surface effect [Mitchell 2013]. The PALS model addresses problems that arise due to missing bonds (see Figure 3) near the surface of a peridynamic body. Using this new model, simple benchmark calculations demonstrate large reductions in the surface effect. Although the development given in the present paper is for linear elastic materials, work currently in progress suggests that previously developed plasticity and viscoelasticity models [Mitchell 2011a; 2011b] can be extended to include some aspects of the PALS approach.

## Acknowledgements

This work was supported through a Laboratory-Directed Research and Development (LDRD) project at Sandia National Laboratories. The authors would like to thank Dan Turner, Pablo Seleson, Mike Parks, and Max Gunzburger for helpful discussions during the course of this work. Sandia is a multiprogram laboratory operated by Sandia Corporation, a Lockheed Martin Company, for the United States Department of Energy under Contract DE-AC04-94AL85000.

## References

- [Bessa et al. 2014] M. A. Bessa, J. T. Foster, T. Belytschko, and W. K. Liu, “A meshfree unification: reproducing kernel peridynamics”, *Comput. Mech.* **53**:6 (2014), 1251–1264.
- [Bonet and Wood 1997] J. Bonet and R. D. Wood, *Nonlinear continuum mechanics for finite element analysis*, Cambridge University Press, 1997. Second edition published in 2008.
- [Cubit 2014] Cubit, “Cubit mesh generation code”, 2014, <http://cubit.sandia.gov>.
- [Foster et al. 2010] J. T. Foster, S. A. Silling, and W. W. Chen, “Viscoplasticity using peridynamics”, *Int. J. Numer. Methods Eng.* **81**:10 (2010), 1242–1258.
- [Kilic 2008] B. Kilic, *Peridynamic theory for progressive failure prediction in homogeneous and heterogeneous materials*, Ph.D. thesis, University of Arizona, Tucson, AZ, 2008.
- [Littlewood  $\geq$  2015] D. J. Littlewood, “Roadmap for software implementation”, in *Handbook of peridynamic modeling*, edited by F. Bobaru et al., Chapman Hall/CRC, Boca Raton, FL. Expected publication 2015.
- [Macek and Silling 2007] R. W. Macek and S. A. Silling, “Peridynamics via finite element analysis”, *Finite Elem. Anal. Des.* **43**:15 (2007), 1169–1178.
- [Madenci and Oterkus 2014] E. Madenci and E. Oterkus, *Peridynamic theory and its applications*, Springer, New York, 2014.
- [Mitchell 2011a] J. A. Mitchell, “A nonlocal, ordinary, state-based plasticity model for peridynamics”, SAND report 2011-3166, Sandia National Laboratories, 2011, <https://cfwebprod.sandia.gov/cfdocs/CompResearch/docs/SAND2011-3166.pdf>.
- [Mitchell 2011b] J. A. Mitchell, “A non-local, ordinary-state-based viscoelasticity model for peridynamics”, SAND report 2011-8064, Sandia National Laboratories, Albuquerque, NM and Livermore, CA, 2011, <https://cfwebprod.sandia.gov/cfdocs/CompResearch/docs/SAND2011-Viscoelasticity.pdf>.
- [Mitchell 2013] J. A. Mitchell, “On the ‘DSF’ and the ‘dreaded surface effect’”, slides of presentation at Workshop on Nonlocal Damage and Failure (San Antonio, TX, 2013), Sandia National Laboratories, 2013, <https://cfwebprod.sandia.gov/cfdocs/CompResearch/docs/SAND2013-1927C.pdf>.
- [ParaView 2014] ParaView, “ParaView visualization code”, 2014, <http://www.paraview.org>.
- [Parks et al. 2012] M. L. Parks, D. J. Littlewood, J. A. Mitchell, and S. A. Silling, “Peridigm users’ guide v1.0.0”, SAND report 2012-7800, Sandia National Laboratories, September 2012, <http://www.osti.gov/scitech/servlets/purl/1055619>.

- [Peridigm 2014] J. Aidun, J. T. Foster, D. J. Littlewood, J. A. Mitchell, M. L. Parks, S. A. Silling, and D. Turner, “Peridigm”, 2014, <http://peridigm.sandia.gov>.
- [Seleson and Parks 2011] P. Seleson and M. L. Parks, “On the role of the influence function in the peridynamic theory”, *J. Multiscale Comput. Eng.* **9**:6 (2011), 689–706.
- [Silling 2000] S. A. Silling, “Reformulation of elasticity theory for discontinuities and long-range forces”, *J. Mech. Phys. Solids* **48**:1 (2000), 175–209.
- [Silling and Askari 2005] S. A. Silling and E. Askari, “A meshfree method based on the peridynamic model of solid mechanics”, *Comput. Struct.* **83**:17–18 (2005), 1526–1535.
- [Silling and Lehoucq 2010] S. A. Silling and R. B. Lehoucq, “Peridynamic theory of solid mechanics”, *Adv. Appl. Mech.* **44** (2010), 73–168.
- [Silling et al. 2007] S. A. Silling, M. Epton, O. Weckner, J. Xu, and E. Askari, “Peridynamic states and constitutive modeling”, *J. Elasticity* **88**:2 (2007), 151–184.
- [Tupek and Radovitzky 2014] M. R. Tupek and R. Radovitzky, “An extended constitutive correspondence formulation of peridynamics based on nonlinear bond-strain measures”, *J. Mech. Phys. Solids* **65** (2014), 82–92.
- [Tupek et al. 2013] M. R. Tupek, J. J. Rimoli, and R. Radovitzky, “An approach for incorporating classical continuum damage models in state-based peridynamics”, *Comput. Methods Appl. Mech. Eng.* **263** (2013), 20–26.

Received 2 Oct 2014. Revised 9 Feb 2015. Accepted 12 Mar 2015.

JOHN A. MITCHELL: [jamitch@sandia.gov](mailto:jamitch@sandia.gov)

Multiscale Science, Sandia National Laboratories, P.O. Box 5800, MS 1322, Albuquerque, NM 87185-1322, United States

STEWART A. SILLING: [sasilli@sandia.gov](mailto:sasilli@sandia.gov)

Multiscale Science, Sandia National Laboratories, P.O. Box 5800, MS 1322, Albuquerque, NM 87185-1322, United States

DAVID J. LITTLEWOOD: [djlittl@sandia.gov](mailto:djlittl@sandia.gov)

Multiscale Science, Sandia National Laboratories, PO Box 5800, MS 1322, Albuquerque, NM 87185-1322, United States



# JOURNAL OF MECHANICS OF MATERIALS AND STRUCTURES

[msp.org/jomms](http://msp.org/jomms)

Founded by Charles R. Steele and Marie-Louise Steele

## EDITORIAL BOARD

ADAIR R. AGUIAR	University of São Paulo at São Carlos, Brazil
KATIA BERTOLDI	Harvard University, USA
DAVIDE BIGONI	University of Trento, Italy
YIBIN FU	Keele University, UK
IWONA JASIUK	University of Illinois at Urbana-Champaign, USA
C. W. LIM	City University of Hong Kong
THOMAS J. PENCE	Michigan State University, USA
DAVID STEIGMANN	University of California at Berkeley, USA

## ADVISORY BOARD

J. P. CARTER	University of Sydney, Australia
D. H. HODGES	Georgia Institute of Technology, USA
J. HUTCHINSON	Harvard University, USA
D. PAMPLONA	Universidade Católica do Rio de Janeiro, Brazil
M. B. RUBIN	Technion, Haifa, Israel

**PRODUCTION** [production@msp.org](mailto:production@msp.org)

SILVIO LEVY Scientific Editor

Cover photo: Wikimedia Commons

---

See [msp.org/jomms](http://msp.org/jomms) for submission guidelines.


---

JoMMS (ISSN 1559-3959) at Mathematical Sciences Publishers, 798 Evans Hall #6840, c/o University of California, Berkeley, CA 94720-3840, is published in 10 issues a year. The subscription price for 2015 is US\$565/year for the electronic version, and \$725/year (+\$60, if shipping outside the US) for print and electronic. Subscriptions, requests for back issues, and changes of address should be sent to MSP.

---

JoMMS peer-review and production is managed by EditFLOW® from Mathematical Sciences Publishers.

PUBLISHED BY

 **mathematical sciences publishers**  
nonprofit scientific publishing

<http://msp.org/>

© 2015 Mathematical Sciences Publishers

## Special issue on Peridynamic Theory

<b>Preface</b>	<b>STEWART A. SILLING and OLAF WECKNER</b>	<b>537</b>
<b>A position-aware linear solid constitutive model for peridynamics</b>	<b>JOHN A. MITCHELL, STEWART A. SILLING and DAVID J. LITTLEWOOD</b>	<b>539</b>
<b>Peridynamics analysis of the nanoscale friction and wear properties of amorphous carbon thin films</b>	<b>SAYNA EBRAHIMI, DAVID J. STEIGMANN and KYRIAKOS KOMVOPOULOS</b>	<b>559</b>
<b>Inverse problems in heterogeneous and fractured media using peridynamics</b>	<b>D. Z. TURNER, B. G. VAN BLOEMEN WAANDERS and M. L. PARKS</b>	<b>573</b>
<b>Variable horizon in a peridynamic medium</b>	<b>STEWART A. SILLING, DAVID J. LITTLEWOOD and PABLO SELESON</b>	<b>591</b>
<b>A dynamic electro-thermo-mechanical model of dielectric breakdown in solids using peridynamics</b>	<b>RAYMOND A. WILDMAN and GEORGE A. GAZONAS</b>	<b>613</b>

